OPTICS

Tunable guided resonance in twisted bilayer photonic crystal

Beicheng Lou[1], Benjamin Wang[2], Jesse A Rodríguez[2], Mark Cappelli[2], Shanhui Fan[3]*

We experimentally demonstrate tunable guided resonance in twisted bilayer photonic crystals. Both the numerically and the experimentally obtained transmission spectra feature resonances with frequencies strongly dependent on the twist angle, as well as resonances with frequencies that are largely independent of the twist angle. These resonant features can be well understood with a simple analytic theory based on band folding. Our work illustrates the rich tunable resonance physics in twisted bilayer systems.

INTRODUCTION

The effect of guided resonance is very prominent in an optical thin-film structure with periodic in-plane refractive index modulations. The modulation results in the phase matching of externally incident plane wave with the guided mode of the thin film, which can lead to strong resonance response and enhanced light-matter interaction (*1*–*3*). Guided resonance has been used in many devices including sensors (*4*–*7*), filters (*8*–*16*), light-emitting diodes (*17*), and lasers (*18*–*22*) and in applications (*23*, *24*) such as image differentiation (*25*–*27*), slow light generation (*28*), and control of thermal emission (*29*).

While the properties of guided resonance can be engineered by structure design, tuning guided resonance after the structure is fabricated remains a challenge. Some previous work relies on perturbing the refractive index of the film (*10*, *30*–*33*), changing the incident angle (*34*), or by using a two-layer structure and changing the interlayer gap size (*35*, *36*). The tuning range of all these techniques in practice is quite limited. In addition, in many applications, one prefers to operate the device at a fixed angle of incidence, for which the change of incident angle is not applicable.

In recent years, there has been much interest in twisted bilayer photonic structures (*37*–*43*). These structures consist of two thin films on top of each other. With proper design of each layer, the optical property of the bilayer system becomes strongly dependent on the twist angle, which can enable applications such as tunable circular dichroism (*40*–*42*), tunable frequency filter (*44*), tunable thermal emission (*45*), and tunable lens focus (*43*). In particular, when both of these layers consist of a periodic structure, for example, when both layers are photonic crystal slabs, the periodicity of the twisted bilayer system becomes strongly dependent on the twist angle because of the moiré effects (*46*–*48*). Because the phase-matching condition of the guided resonance with the external plane wave depends strongly on the periodicity, the frequency of guided resonance can become strongly dependent on the twist angle. This effect of using twist angle to tune guided resonance has been recently studied theoretically (*46*), but there has not been an experimental demonstration. Moreover, the previous theoretical study assumes that each layer is infinitely periodic within the layer. From the previous study, it remains unclear how the effects may be in practical structures where each layer necessarily has a finite spatial extent.

Here, we provide an experimental study of twisted bilayer photonic crystal slabs in the microwave frequency range, as illustrated in Fig. 1. We show that the guided resonances can be highly tunable by twist angle. The measured transmission spectrum agree well with both the simplified theory and the rigorous coupled wave analyses. It is a demonstration of tuning guided resonance in photonic crystal slabs by twist angle and points to the substantial opportunities in exploiting these structures in device applications.

RESULTS

Theory

In general, to the lowest-order approximation, the properties of guided resonance of a photonic crystal slab can be understood from a band folding picture starting from the guided mode band structure of the corresponding uniform slab (*1*). In our experimental structure, the total thickness of the two-layer structure is 0.73 cm, and the operating wavelength is around 1 cm. Therefore, the corresponding uniform slab is in the single-mode regime, as characterized by a single-band $\omega_{\text{eff}}(\mathbf{k})$.

For a wave incident onto the photonic crystal slab, with an in-plane wave vector $\mathbf{k}_{\text{inc}}$, the frequency of the excited guided resonance can be approximated as

$$\omega_g = \omega_{\text{eff}}(\mathbf{k}_{\text{inc}} + \mathbf{g}) \tag{1}$$

where $\mathbf{g}$ is a reciprocal lattice vector. At a nonzero twist angle, our structure in Fig. 1A forms a two-dimensional (2D) lattice as shown in Fig. 1B, with lattice vectors $\mathbf{a}_1 = a\hat{\mathbf{y}}'/\sin\alpha$ and $\mathbf{a}_2 = a\hat{\mathbf{y}}/\sin\alpha$ along the rods in the two layers, where a is the lattice constant of each layer, $\hat{\mathbf{y}}$ is the unit vector along the rods in the first layer, and $\hat{\mathbf{y}}'$ is the unit vector $\hat{\mathbf{y}}$ rotated by angle α to be along the rods in the second layer. The corresponding reciprocal lattice is then

$$\mathcal{G}_2 \equiv \{\mathbf{g}: \mathbf{g} = 2n\pi\hat{\mathbf{x}}/a + 2n'\pi\hat{\mathbf{x}}'/a, n, n' \in \mathbb{Z}\} \tag{2}$$

where $\hat{\mathbf{x}}$ and $\hat{\mathbf{x}}'$ are unit vectors perpendicular to the rods in each layer, respectively. Alternatively, the reciprocal lattice can be understood from a multilayer scattering picture. Incident plane wave with in-plane wave vector $\mathbf{k}_{\text{inc}}$ passing through the first layer will be scattered into plane waves of wave vectors $\{\mathbf{k}_{\text{inc}} + 2n\pi\hat{\mathbf{x}}/a: n \in \mathbb{Z}\}$, which

[1]Department of Applied Physics, Stanford University, Stanford, CA 94305, USA. [2]Department of Mechanical Engineering, Stanford University, Stanford, CA 94305, USA. [3]Department of Electrical Engineering, Stanford University, Stanford, CA 94305, USA.
*Corresponding author. Email: shanhui@stanford.edu.

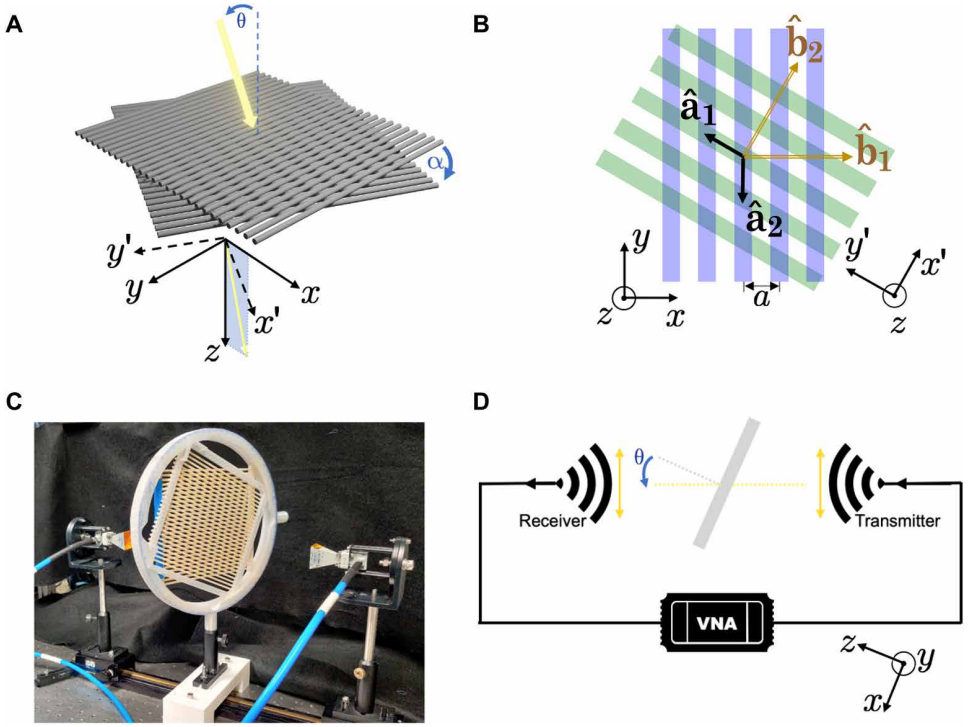

Fig. 1. Illustration of the experiment setup. (**A**) Diagram of a twisted bilayer structure interacting with incident light. The *y* and *y*′ axes are along the rods in the two layers. (**B**) The lattice vectors of the real space ($\hat{\mathbf{a}}_1$, $\hat{\mathbf{a}}_2$) and of the reciprocal space ($\hat{\mathbf{b}}_1$, $\hat{\mathbf{b}}_2$) for the twisted bilayer structure shown in (A). (**C**) Photo of the experiment structure taken in the laboratory. (**D**) Measurement scheme where two horn antennas are placed on the two sides of the structure and connected to a vector network analyzer (VNA).

will be further scattered by the second layer into plane waves of wave vectors $\{\mathbf{k}_{\text{inc}} + 2n\pi\hat{\mathbf{x}}/a + 2n'\pi\hat{\mathbf{x}}'/a: n, n' \in \mathbb{Z}\}$, i.e., $\{\mathbf{k}_{\text{inc}} + \mathbf{g}: \mathbf{g} \in \mathcal{G}_2\}$.

Different choice of $\mathbf{g}$ in Eq. 1 gives rise to different dependencies of the resonant frequency on the twist angle. The choice of either $n = 0$ or $n' = 0$ gives rise to resonances that are almost independent of the twist angle. The two lowest-order angle-independent resonances have frequencies

$$\omega_1 = \omega_{\text{eff}}(\mathbf{k}_{\text{inc}} \pm 2\pi\hat{\mathbf{x}}/a) = \omega_{\text{eff}}(\mathbf{k}_{\text{inc}} \pm 2\pi\hat{\mathbf{x}}'/a) \quad (3)$$

$$\omega_2 = \omega_{\text{eff}}(\mathbf{k}_{\text{inc}} \pm 4\pi\hat{\mathbf{x}}/a) = \omega_{\text{eff}}(\mathbf{k}_{\text{inc}} \pm 4\pi\hat{\mathbf{x}}'/a) \quad (4)$$

These are guided resonances associated with the periodicity of one of the layers. On the other hand, when both n and n' are not zero, the frequencies of the resulting guided resonance becomes highly dependent on the twist angle. The two lowest orders of these twist angle–dependent resonances have the frequencies

$$\begin{aligned}\omega_3 &= \omega_{\text{eff}}(\mathbf{k}_{\text{inc}} \pm 2\pi(\hat{\mathbf{x}} - \hat{\mathbf{x}}')/a) \\ &= \omega_{\text{eff}}(\mathbf{k}_{\text{inc}} \pm 2\pi((1 - \cos\alpha)\hat{\mathbf{x}} + \sin\alpha\,\hat{\mathbf{y}})/a)\end{aligned} \quad (5)$$

$$\begin{aligned}\omega_4 &= \omega_{\text{eff}}(\mathbf{k}_{\text{inc}} \pm 2\pi(2\hat{\mathbf{x}} - \hat{\mathbf{x}}')/a) \\ &= \omega_{\text{eff}}(\mathbf{k}_{\text{inc}} \pm 2\pi((2 - \cos\alpha)\hat{\mathbf{x}} + \sin\alpha\,\hat{\mathbf{y}})/a)\end{aligned} \quad (6)$$

From Eqs. 5 and 6, we can also see the connection of these twist angle–dependent resonances to the moiré wave vector $\mathbf{g}_{\text{m}}(\alpha) \equiv 2\pi(\hat{\mathbf{x}} - \hat{\mathbf{x}}')/a$ (*46*). The tunability of these resonances is directly related to the strong dependency of the moiré wave vector on the twist angle, as illustrated in Fig. 2.

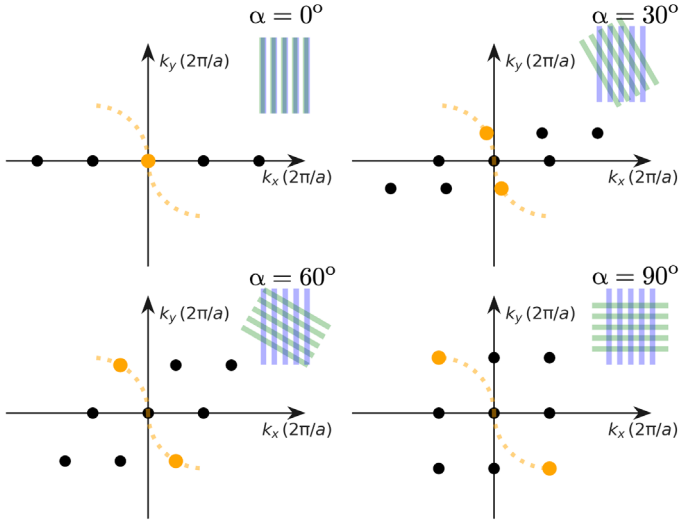

Fig. 2. Variation of the reciprocal lattice bases as the twist angle is varied, with the lowest-order moiré wave vector $\pm\mathbf{g}_{\text{m}}(\alpha)$traced out by the orange line as a function of twist angle.

At normal incidence, $\mathbf{k}_{\text{inc}} = 0$ and the wave vector arguments for ω_{eff} in Eqs. 3 to 6 have twist angle dependence shown in Fig. 3A. The choice of sign results in two dashed lines for each color. The

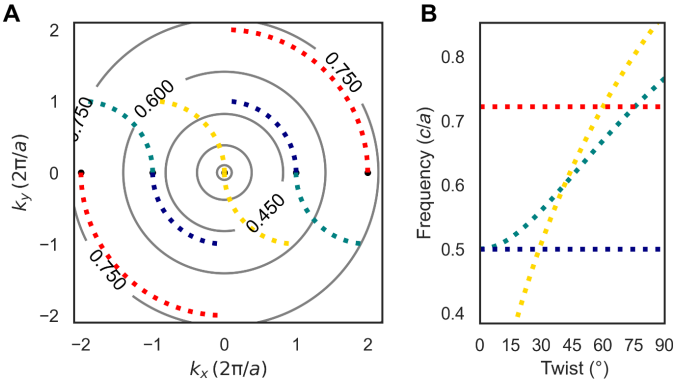

Fig. 3. The origin of angle-dependent and angle-independent resonant frequencies. (**A**) The contour lines are the frequencies of the guided modes in an effective uniform slab as a function of wave vectors. The slab has a thickness of 1.14*a*, where *a* is the lattice constant for individual layers, and a dielectric constant of $\varepsilon_r = 5.7$. The frequencies are in the unit of *c*/*a*, where *c* is the speed of light. The dashed colored lines are the wave vectors of various guided resonances that couple to normally incident light at various twist angles. (**B**) The resonant frequencies of the twisted system as a function of twist angle for the various wave vectors shown as dashed lines in (A).

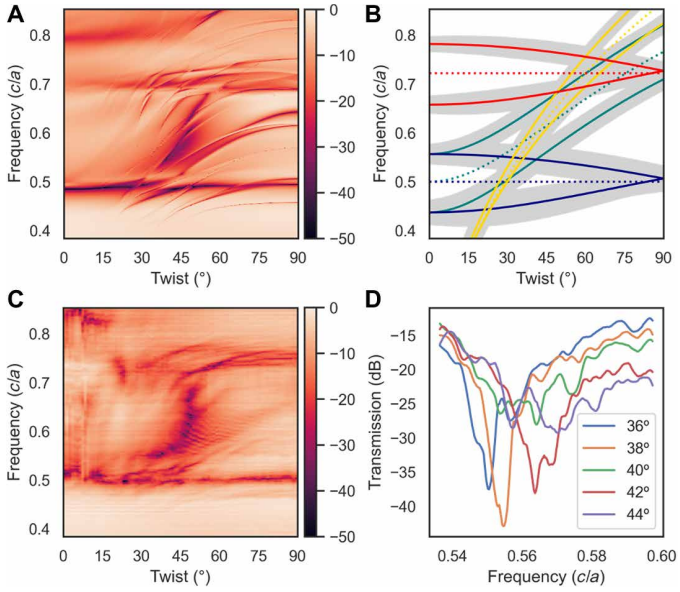

Fig. 4. Transmission of linearly polarized light at incident angle θ = 26.6°, as a function of frequency and twist angle. The numerical calculation from rigorous coupled-wave analysis is shown in (**A**). The theoretical prediction using the lowest-order moiré wave vector is provided for reference in (**B**). Dotted lines are the resonant frequencies for normal incidence. Solid lines are the resonant frequencies for off-normal incidence. Notice the lifting of some of the degeneracies as one moves from normal to off-normal incidence. The experimental measurement is shown in (**C**). The transmission spectra at a few twist angles (36°, 38°, 40°, 42°, and 44°), showing angle dependence of the guided resonance frequency, are collected in (**D**).

corresponding resonant frequencies, also as a function of twist angle, is shown in Fig. 3B. Each dashed line represents a doubly degenerate resonance, for the two choices of sign in Eqs. 5 and 6.

Transmission simulation and measurement

For our experimental structure, we first show in Fig. 4A the transmission spectra as obtained from the rigorous coupled wave analysis. The color indicates the transmitted power of linearly polarized light in the zeroth diffraction order in log scale. There are a large number of transmission spikes and dips, indicating a large number of guided resonances. While most resonances have twist angle–dependent frequencies, there are two sets of resonances that are largely twist angle–independent, around the frequencies 0.50 *c*/*a* and 0.71 *c*/*a*. The transmission spectra for the case of normal incidence can be found in section S1.

To better understand the results from the numerical simulations, we show the theoretically predicted resonant frequencies using Eqs. 3 to 6 as a function of twist angle in Fig. 4B. We note that this theory simply takes as input the band structure of an effective uniform slab and then estimates the resonant frequency by wave vector matching consideration only. This theory does not take into account any scattering or coupling effects from the grating. A more elaborate theory on the resonances can be developed following (*46*). Here, the dashed lines each are a doubly degenerate resonance as in Fig. 3B, corresponding to $\mathbf{k}_{inc} = 0$. In our experiment, because the incoming light is at an incident angle θ = 26.6°, $\mathbf{k}_{inc} \neq 0$ and the degeneracies of the resonances are lifted, as shown by the solid lines in Fig. 4B. Moreover, because the incident beam has a transverse Gaussian profile, deviating from the plane wave assumption, there will be a broadening of the predicted resonant frequencies, as shown by the gray shades in Fig. 4B. Specifically, if we denote the Gaussian beam width as *W*, i.e., the transverse power distribution of the beam $P(x, y) \propto e^{-(x^2+y^2)/W^2}$, then the gray shades in Fig. 4B correspond to resonant frequencies for wave vectors $\{\mathbf{k}_{inc} + \delta\mathbf{k} : |\delta\mathbf{k}| < 2\pi/W\}$, as also obtained from Eqs. 3 to 6. The theoretical prediction is based on $\omega_{eff}(\mathbf{k}) = 0.5\,|\mathbf{k}|^{0.53}$. This parametric form is chosen to account for the band dispersion in photonic crystals and is obtained by fitting to the band structure of the bilayer structure at α = 0° within the frequency range of interest. All four pairs of bands in Fig. 4B could be identified with corresponding transmission spikes and dips in Fig. 4A, despite a slight difference in dispersion.

The experimental measurement of transmission spectrum at various twist angles is shown in Fig. 4C. The color indicates the transmitted power of linearly polarized light, with the polarization aligned to $\hat{\mathbf{x}}$, in the zeroth diffraction order in log scale. The measured transmission as a function of frequency and twist angle has various sharp variations that reveal the corresponding guided resonances. There are two sets of transmission dips around frequencies 0.50 *c*/*a* and 0.71 *c*/*a* that are largely independent of the twist angle. They correspond to the guided resonance modes shown as red and blue in Fig. 4B, where the degeneracy is lifted because of off-normal incidence. There are also two sets of resonant features that are highly dependent on the twist angle. One of them has the resonant frequencies varying from 0.50 *c*/*a* to 0.65 *c*/*a* as the angle varies from 0° to 90°. The other has the frequencies varying from 0.55 *c*/*a* to 0.65 *c*/*a* as the twist angle varies from 45° to 50°. They correspond to the guided resonance modes shown as green and yellow in Fig. 4B. The experiment result matches the simulation reasonably well, despite showing fewer resonances than the simulation. This is expected because we are using a finite structure that cannot manifest the modes with sufficiently high-quality factors, while the simulation assumes infinite structure. All four sets of bands from the theory prediction based on low-order scattering processes are visible, indicating the

robustness of these processes and the applicability of the low-order model. The highly tunable guided resonance mode from theory prediction (green line in Fig. 4B) is not completely visible in the numerical result (Fig. 4A) because many other resonances corresponding to higher-order processes cut across it as the twist angle is varied. However, it has an excellent match in the experiment result where high-order processes are less visible because of finite size, which further motivates the low-order model. To see the tunable guided resonances more clearly, we also show the transmission spectra between 0.54 c/a and 0.60 c/a for a few twist angles in Fig. 4D. Here, the transmission spectra are smoothened, and one can see the clear presence of resonance features that are strongly tunable by the twist angle. The transmissions are all below −15 dB because the chosen frequency range is near resonance. In fig. S3, we provide the experimental transmission spectra at the same twist angles but over a larger frequency range. From these plots, we see that the experimental insertion loss is actually small. More details of the resonance features can be found in sections S2 to S4.

DISCUSSION

We experimentally demonstrate tunable guided resonance in twisted bilayer photonic crystals. Both the numerically and the experimentally obtained transmission spectra feature resonances with frequencies strongly dependent on the twist angle, as well as resonances with frequencies that are largely independent of the twist angle. These resonant features can be well understood with a simple analytic theory based on band folding. The transmission spectrum from rigorous coupled wave analysis have richer details than the experimental measurements, but many features can be matched between the two, which is remarkable given the small extent of our experimental structure. Our work illustrates the rich tunable resonance physics in twisted bilayer systems.

MATERIALS AND METHODS

Experimental setup

Our experiment structure consists of two layers of alumina rod arrays, as illustrated in Fig. 1A. The alumina rods are held by a 3D printed scaffold using polylactide (PLA) at low filling ratio, as shown in Fig. 1C. The alumina rods have a dielectric constant $\varepsilon_r = 9.8$ and a radius of $r = 0.17$ cm, while the PLA scaffold has a dielectric constant less than 2. The layers have a lattice constant of $a = 0.64$ cm and an interlayer gap spacing of 0.05 cm. With our setup, the in-plane twist angle can vary continuously from 0° to 90°. A pair of horn antennas, with operating frequencies spanning multiple octaves between 18 and 40GHz, are placed on the two sides of the twisted structure and connected to a vector network analyzer, as illustrated in Fig. 1D. The vector network analyzer measures the transmission of a linearly polarized (along x axis) microwave beam with a Gaussian profile in the transverse direction. The Gaussian beam spans across a range of approximately 10 cm and does not directly see the edge of the structure. The incident angle is set at $\theta = 26.6°$ to eliminate multiple reflections between the ports and the structure. We aim to measure the transmission in the zeroth diffraction order while continuously varying the twist angle α.

SUPPLEMENTARY MATERIALS

Supplementary material for this article is available at https://science.org/doi/10.1126/sciadv.add4339

REFERENCES AND NOTES

1. S. Fan, J. D. Joannopoulos, Analysis of guided resonances in photonic crystal slabs. *Phys. Rev. B* **65**, 235112 (2002).
2. A. Hessel, A. A. Oliner, A new theory of wood's anomalies on optical gratings. *Appl. Optics* **4**, 1275–1297 (1965).
3. R. Magnusson, S. S. Wang, New principle for optical filters. *Appl. Phys. Lett.* **61**, 1022–1024 (1992).
4. P. K. Sahoo, S. Sarkar, J. Joseph, High sensitivity guided-mode-resonance optical sensor employing phase detection. *Sci. Rep.* **7**, 7607 (2017).
5. M. Pan, Z. Liang, Y. Wang, Y. Chen, Tunable angle-independent refractive index sensor based on Fano resonance in integrated metal and graphene nanoribbons. *Sci. Rep.* **6**, 29984 (2016).
6. G. J. Triggs, Y. Wang, C. P. Reardon, M. Fischer, G. J. O. Evans, T. F. Krauss, Chirped guided-mode resonance biosensor. *Optica* **4**, 229–234 (2017).
7. W. Zhou, D. Zhao, Y.-C. Shuai, H. Yang, S. Chuwongin, A. Chadha, J.-H. Seo, K. X. Wang, V. Liu, Z. Ma, S. Fan, Progress in 2d photonic crystal fano resonance photonics. *Prog. Quantum Electron.* **38**, 1–74 (2014).
8. A. K. Kodali, M. Schulmerich, J. Ip, G. Yen, B. T. Cunningham, R. Bhargava, Narrowband midinfrared reflectance filters using guided mode resonance. *Anal. Chem.* **82**, 5697–5706 (2010).
9. P. T. Dang, K. Q. Le, Q. M. Ngo, H. P. T. Nguyen, T. K. Nguyen, Guided-mode resonance filter with ultra-narrow bandwidth over the visible frequencies for label-free optical biosensor. *J. Adv. Eng. Comput.* **3**, 406–414 (2019).
10. D. W. Dobbs, B. T. Cunningham, Optically tunable guided-mode resonance filter. *Appl. Optics* **45**, 7286–7293 (2006).
11. H. S. Bark, T.-I. Jeon, Tunable terahertz guided-mode resonance filter with a variable grating period. *Opt. Express* **26**, 29353–29362 (2018).
12. L. Macé, O. Gauthier-Lafaye, A. Monmayrant, S. Calvez, H. Camon, H. Leplan, Highly-resonant two-polarization transmission guided-mode resonance filter. *AIP Adv.* **8**, 115228 (2018).
13. N. Saha, W.-K. Kou, Guided-mode resonance-based bandpass filter operating at full conical mounting. *Appl. Optics* **59**, 10700–10705 (2020).
14. M. Barrow, J. Phillips, Polarization-independent narrowband transmittance filters via symmetry-protected modes in high contrast gratings. *Opt. Lett.* **45**, 4348–4351 (2020).
15. S. Luo, L. Chen, Y. Bao, N. Yang, Y. Zhu, Non-polarizing guided-mode resonance grating filter for telecommunications. *Optik* **124**, 5158–5160 (2013).
16. J.-N. Liu, M. V. Schulmerich, R. Bhargava, B. T. Cunningham, Optimally designed narrowband guided-mode resonance reflectance filters for mid-infrared spectroscopy. *Opt. Express* **19**, 24182–24197 (2011).
17. A. Shakoor, R. Lo Savio, P. Cardile, S. L. Portalupi, D. Gerace, K. Welna, S. Boninelli, G. Franzò, F. Priolo, T. F. Krauss, M. Galli, L. O'Faolain, Room temperature all-silicon photonic crystal nanocavity light emitting diode at sub-bandgap wavelengths. *Laser Photonics Rev.* **7**, 114–121 (2013).
18. K. Hirose, Y. Liang, Y. Kurosaka, A. Watanabe, T. Sugiyama, S. Noda, Watt-class high-power, high-beam-quality photonic-crystal lasers. *Nat. Photonics* **8**, 406–411 (2014).
19. R. Morita, T. Inoue, M. De Zoysa, K. Ishizaki, S. Noda, Photonic-crystal lasers with two-dimensionally arranged gain and loss sections for high-peak-power short-pulse operation. *Nat. Photonics* **15**, 311–318 (2021).
20. A. Y. Song, A. R. K. Kalapala, W. Zhou, S. Fan, First-principles simulation of photonic crystal surface-emitting lasers using rigorous coupled wave analysis. *Appl. Phys. Lett.* **113**, 041106 (2018).
21. M. Notomi, H. Suzuki, T. Tamamura, K. Edagawa, Lasing action due to the two-dimensional quasiperiodicity of photonic quasicrystals with a penrose lattice. *Phys. Rev. Lett.* **92**, 123906 (2004).
22. N. Takemura, M. Takiguchi, E. Kuramochi, A. Shinya, T. Sato, K. Takeda, S. Matsuo, M. Notomi, Lasing thresholds and photon statistics in high-β buried multiple quantum well photonic crystal nanocavity lasers. *Phys. Rev. A* **99**, 053820 (2019).
23. M. E. Beheiry, V. Liu, S. Fan, O. Levi, Sensitivity enhancement in photonic crystal slab biosensors. *Opt. Express* **18**, 22702–22714 (2010).
24. F. Priolo, T. Gregorkiewicz, M. Galli, T. F. Krauss, Silicon nanostructures for photonics and photovoltaics. *Nat. Nanotechnol.* **9**, 19–32 (2014).
25. C. Guo, M. Xiao, M. Minkov, Y. Shi, S. Fan, Photonic crystal slab laplace operator for image differentiation. *Optica* **5**, 251–256 (2018).
26. H. Kwon, D. Sounas, A. Cordaro, A. Polman, A. Alù, Nonlocal metasurfaces for optical signal processing. *Phys. Rev. Lett.* **121**, 173004 (2018).
27. Y. Zhou, H. Zheng, I. I. Kravchenko, J. Valentine, Flat optics for image differentiation. *Nat. Photonics* **14**, 316–323 (2020).
28. J. D. de Pineda, G. P. Ward, A. P. Hibbins, J. R. Sambles, Metasurface bilayer for slow microwave surface waves. *Phys. Rev. B* **100**, 081409 (2019).
29. M. Ghebrebrhan, P. Bermel, Y. X. Yeng, I. Celanovic, M. Soljačić, J. D. Joannopoulos, Tailoring thermal emission via Q matching of photonic crystal resonances. *Phys. Rev. A* **83**, 033810 (2011).

30. H.-S. Lee, J. Y. Kwak, T.-Y. Seong, G. W. Hwang, W. M. Kim, I. Kim, K.-S. Lee, Optimization of tunable guided-mode resonance filter based on refractive index modulation of graphene. *Sci. Rep.* **9**, 19951 (2019).
31. R. Magnusson, M. Shokooh-Saremi, Widely tunable guided-mode resonance nanoelectromechanical rgb pixels. *Opt. Express* **15**, 10903–10910 (2007).
32. A. Taheri, M. Shokooh-Saremi, Tunable two-dimensional optical filter based on guided-mode resonance. *J. Opt. Soc. Am. A* **36**, 1109–1116 (2019).
33. H. Ichikawa, H. Kikuta, Dynamic guided-mode resonant grating filter with quadratic electro-optic effect. *J. Opt. Soc. Am. A* **22**, 1311–1318 (2005).
34. R. Yukino, P. K. Sahoo, J. Sharma, T. Takamura, J. Joseph, A. Sandhu, Wide wavelength range tunable one-dimensional silicon nitride nano-grating guided mode resonance filter based on azimuthal rotation. *AIP Adv.* **7**, 015313 (2017).
35. H. Y. Song, S. Kim, R. Magnusson, Tunable guided-mode resonances in coupled gratings. *Opt. Express* **17**, 23544–23555 (2009).
36. W. Suh, M. F. Yanik, O. Solgaard, S. Fan, Displacement-sensitive photonic crystal structures based on guided resonance in photonic crystal slabs. *Appl. Phys. Lett.* **82**, 1999–2001 (2003).
37. G. Hu, Q. Ou, G. Si, Y. Wu, J. Wu, Z. Dai, A. Krasnok, Y. Mazor, Q. Zhang, Q. Bao, C.-W. Qiu, A. Alù, Topological polaritons and photonic magic angles in twisted α-MoO_3 bilayers. *Nature* **582**, 209–213 (2020).
38. G. Hu, M. Wang, Y. Mazor, C.-W. Qiu, A. Alù, Tailoring light with layered and moiré metasurfaces. *Trends Chem.* **3**, 342–358 (2021).
39. Z. Wu, Y. Liu, E. H. Hill, Y. Zheng, Chiral metamaterials via Moiré stacking. *Nanoscale* **10**, 18096–18112 (2018).
40. Z. Wu, Y. Zheng, Moiré chiral metamaterials. *Adv. Opt. Mater.* **5**, 1700034 (2017).
41. O. Aftenieva, M. Schnepf, B. Mehlhorn, T. A. F. König, Tunable circular dichroism by photoluminescent moiré gratings. *Adv. Opt. Mater.* **9**, 2001280 (2021).
42. J. Chi, H. Liu, Z. Wang, N. Huang, Giant optical activity in plasmonic chiral structure via double-layer graphene moiré stacking in mid-infrared region. *Opt. Express* **28**, 4529–4540 (2020).
43. S. Bernet, W. Harm, M. Ritsch-Marte, Demonstration of focus-tunable diffractive moiré-lenses. *Opt. Express* **21**, 6955–6966 (2013).
44. B. Lou, S. Fan, Tunable frequency filter based on twisted bilayer photonic crystal slabs. *ACS Photonics* **9**, 800–805 (2022).
45. C. Guo, Y. Guo, B. Lou, S. Fan, Wide wavelength-tunable narrow-band thermal radiation from moiré patterns. *Appl. Phys. Lett.* **118**, 131111 (2021).
46. B. Lou, N. Zhao, M. Minkov, C. Guo, M. Orenstein, S. Fan, Theory for twisted bilayer photonic crystal slabs. *Phys. Rev. Lett.* **126**, 136101 (2021).
47. K. Dong, T. Zhang, J. Li, Q. Wang, F. Yang, Y. Rho, D. Wang, C. P. Grigoropoulos, J. Wu, J. Yao, Flat bands in magic-angle bilayer photonic crystals at small twists. *Phys. Rev. Lett.* **126**, 223601 (2021).
48. H. Tang, F. Du, S. Carr, C. DeVault, O. Mello, E. Mazur, Modeling the optical properties of twisted bilayer photonic crystals. *Light Sci. Appl.* **10**, 157 (2021).

Acknowledgments
Funding: This work is supported by a MURI project from the U.S. Air Force Office of Scientific Research (grant no. FA9550-21-1-0312). **Author contributions:** B.L. and B.W. conceived the idea. B.L., B.W., and J.A.R. performed the experiment, with input from M.C. B.L. performed the numerical simulations and theoretical analysis, with input from S.F. M.C. and S.F. supervised the project. All authors contributed to analyzing the result and writing the manuscript. **Competing interests:** The authors declare that they have no competing interests. **Data and materials availability:** All data needed to evaluate the conclusions in the paper are present in the paper and/or the Supplementary Materials.

Submitted 10 June 2022
Accepted 12 October 2022
Published 30 November 2022
10.1126/sciadv.add4339